

pubs.acs.org/crt Article

Cellular Interactions and Fatty Acid Transporter CD36-Mediated Uptake of Per- and Polyfluorinated Alkyl Substances (PFAS)

Michelle Camdzic, Diana S. Aga, and G. Ekin Atilla-Gokcumen*



Cite This: Chem. Res. Toxicol. 2022, 35, 694–702



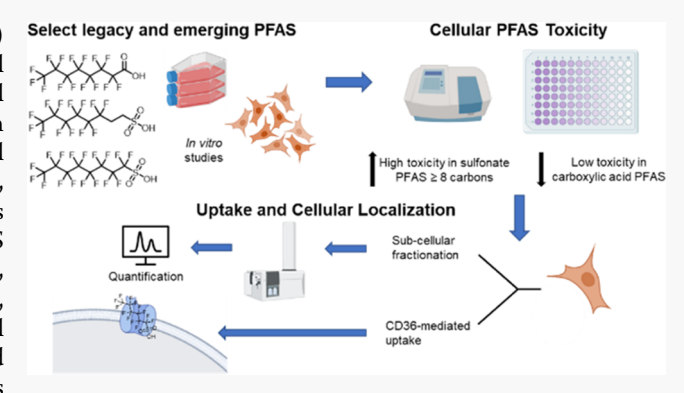
ACCESS

Metrics & More

Article Recommendations

SI Supporting Information

ABSTRACT: Per- and polyfluorinated alkyl substances (PFAS) are a class of widely used compounds in an array of commercial and industrial applications. Due to their extensive use and chemical stability, PFAS persist in the environment and bioaccumulate in humans and wildlife. PFAS exposure have been linked to several negative health effects, including the formation of various cancers, disruption of the endocrine system, and obesity. However, there is a major gap in understanding how structural differences in PFAS impact their interactions within a biological system. In this study, we examined the toxicity of PFAS with differences in chain length, head group, and degree of fluorination in human retinal epithelial cells. We focused on fluorotelomeric and fully fluorinated sulfonates and carboxylates and measured their uptake. Our results



showed that sulfonates are taken up at higher levels as compared to their fluorotelomer and carboxylate counterparts. Furthermore, PFAS with 8 and 10 carbons (C8 and C10) are taken up at a higher level compared to those with six carbons (C6). We also investigated the role of the fatty acid transporter CD36 in PFAS uptake and found that increased CD36 levels result in higher levels of PFAS in cells. Overall, our results suggest that the head group structure of PFAS impacts toxicity, with sulfonates inducing a higher decrease in cell viability (~50%) than carboxylates. Our results also link the activity of CD36 to PFAS uptake into cells.

■ INTRODUCTION

Per- and polyfluorinated alkyl substances (PFAS) are a group of compounds used as coatings in a number of commercial and industrial applications such as fire extinguishing foams, cleaning products, and food packaging.2 They are also used in a variety of consumer products such as cookware, sports clothing, and cosmetics.³ They have been manufactured and used extensively since the 1940s.⁴ PFAS are classified by their fluorinated alkyl chains bearing a number of C-F linkages. They contain a wide range of head groups including sulfonic acid, carboxylic acid, and alcohol groups among others (Figure 1).5 Even though it has long been shown that they persist in the environment due to their chemical stability, it was not until 1968 when fluorinated compounds were first reported in human blood serum.⁶ With their half-lives ranging from a few months to several years, 7,8 PFAS have been found in the blood serum of almost the entire worldwide population, including the United States. 9,10 For example, perfluorobutane sulfonic acid (PFBS) has a half-life of ~46 days, 11 while perfluorooctane sulfonic acid (PFOS) and perfluorohexane sulfonic acid (PFHxS) have half-lives of 5.5 and 8.5 years, respectively. PFAS have also been detected in other biofluids including breastmilk¹² and in different tissues such as liver, kidney, heart, brain, and lungs.¹³ A recent study has also reported PFAS in human fetal organs.14

Studies have revealed a myriad of health issues associated with PFAS exposure. It has been found that PFAS can cause disruptions in metabolism, which can lead to weight gain, especially in women. The two most widely studied PFAS, PFOS and perfluorooctanoic acid (PFOA), have been associated with decreased fertility in women and in male mice. In addition to these fully fluorinated PFAS, fluorotelomer PFAS (Figure 1A) also exist in the environment. Studies on these fluorotelomers have mainly focused on their effect on marine organisms, which facilitated a growth in interest in their adverse effects in humans.

Based on these *in vivo* observations of adverse effects and bioaccumulation of PFAS, *in vitro* studies were conducted to better understand the effects of PFAS exposure on biological systems. PFAS can interact with various biomolecules including membranes, ²¹ transporters, ²² and other proteins. ²³ These interactions can lead to multiple mechanisms of toxicity and cause PFAS to exhibit different effects and degrees of

Received: March 8, 2022 Published: April 5, 2022





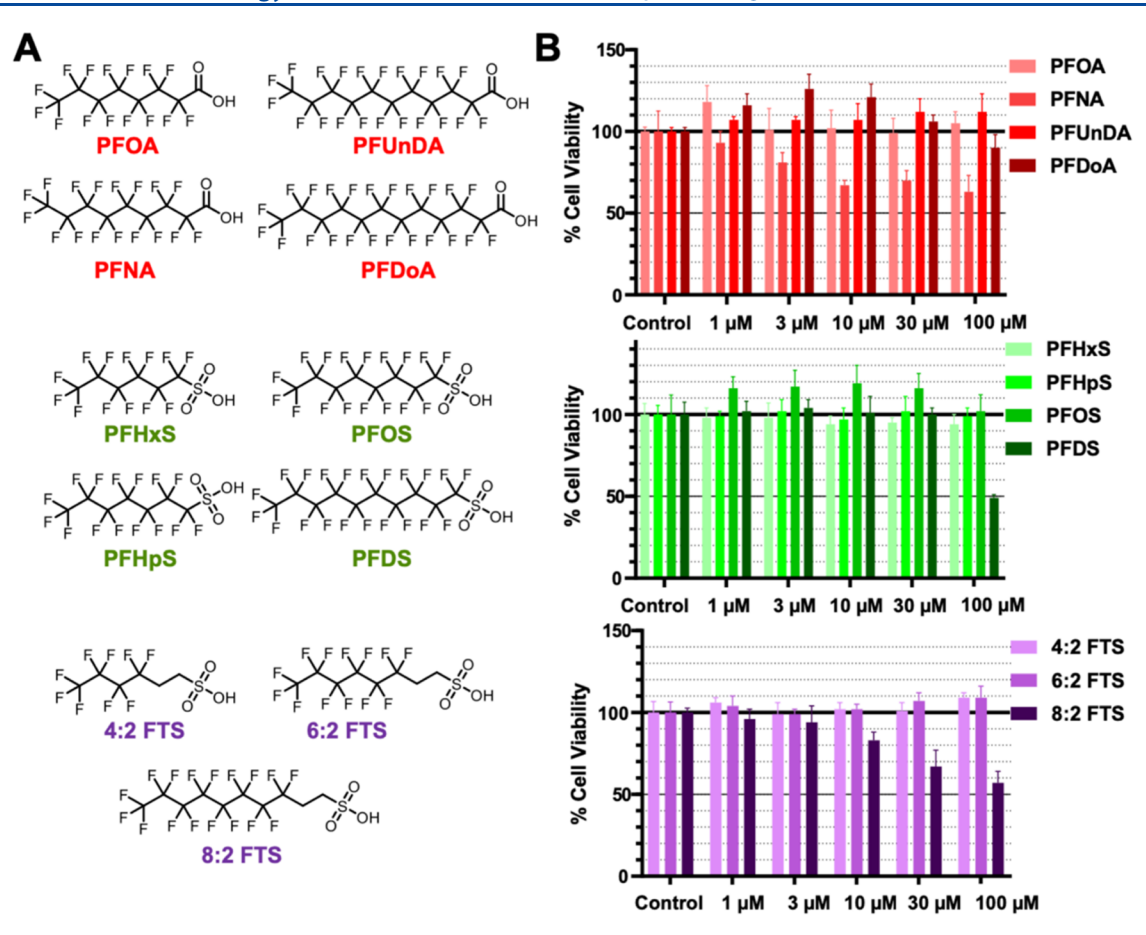


Figure 1. PFAS tested in this study and their effects on cell viability. (A) The structures of carboxylate (perfluorooctanoic acid (PFOA), perfluorononanoic acid (PFNA), perfluoroundecanoic acid (PFUnDA), perfluorododecanoic acid (PFDoA)), sulfonate (PFHxS, perfluoroheptane sulfonic acid (PFHpS), PFOS, perfluorodecane sulfonic acid (PFDS)), and fluorotelomer (4:2 fluorotelomer sulfonic acid (FTS), 6:2 FTS, 8:2 FTS) PFAS tested in this study. (B) 3-(4,5-Dimethylthiazol-2-yl)-2,5-diphenyltetrazolium bromide (MTT) assay results for human retinal epithelium (hTERT RPE-1) cells treated with 1–100 μ M PFAS. Cells were plated overnight on a 96-well plate and incubated at 37 °C. After 24 h, cells were treated with various concentrations of PFAS individually for 24 h. After 24 h of PFAS treatment, MTT was added and incubated at 37 °C for 2.5 h (n = 5 for each treatment condition). Cell viability is reported as a percentage of MeOH vehicle-treated cells (see Table S1 for individual values).

bioaccumulation depending on their precise chemical structures. For example, PFOS promotes cell proliferation at low concentrations (up to $10~\mu M$) but induces toxicity at high concentrations (>200 μM) in human breast epithelial cells. Similarly, carboxylate PFAS strongly induce toxicity in liver cells with EC₅₀ = ~250 μM and show low clearance rates, supporting the bioaccumulative nature of these PFAS. It has also been shown that for carboxylate PFAS, there is a positive correlation between their chain length and toxicity, clearance rate, and subsequent bioaccumulation. However, very few studies systematically evaluated the cytotoxic effects and cellular uptake of PFAS based on varying chain length, head group, and degree of fluorination.

In this work, motivated by the negative health effects of PFAS, we studied the effect of these compounds on cell viability and their molecular interactions. We used a series of PFAS with varying chain lengths, fluorination states, and head group and investigated their *in vitro* toxicity using cell viability assays. We measured the cellular uptake of a select group of PFAS, including fluorotelomer sulfonates and their corresponding fully fluorinated versions and carboxylate counterparts. Among these series of PFAS that we tested, which contained 6, 8, and 10 carbons, longer-chained PFAS exhibited higher levels of cellular uptake. These results prompted us to

investigate the effect of active transport on PFAS uptake. We focused on the involvement of the fatty acid transporter, CD36, which has been previously linked to the bioactivity of PFAS, ³⁰ in the mechanism of PFAS uptake. Increased levels of CD36 resulted in higher cellular levels of PFAS, which was reversed by the pharmacological inhibition of CD36. Overall, our findings show that the cellular uptake of PFAS can vary based on their chain length and fluorination state. Our results also suggest that CD36 may be involved in the uptake of certain PFAS into cells.

MATERIALS AND METHODS

Materials. Human retinal epithelium (hTERT RPE-1) and human embryonic kidney epithelium (HEK-293T) were purchased from the American Type Culture Collection (Manassas, Virginia). Dulbecco's modified Eagle's medium (DMEM), Dulbecco's modified Eagle's medium/nutrient mixture F-12 (DMEM/F-12), fetal bovine serum (FBS), penicillin, streptomycin, and trypsin were purchased from Corning (Corning, NY). BD Difco Luria-Bertani (LB) broth and granulated agar were purchased from Fisher Scientific (Waltham, MA).

E.Z.N.A. plasmid DNA Midi Kit was purchased from Omega Bio-Tek (Norcross, GA). FusionRed-CD36 plasmid was obtained from Addgene and extracted from the previously prepared bacterial pellets using the instructions provided in the kit. Mouse monoclonal anti- α -

tubulin antibody was purchased from Sigma-Aldrich (St. Louis, MO), and rabbit polyclonal anti-CD36 antibody was purchased from Thermo Fisher Scientific (Waltham, MA). Goat antirabbit horseradish peroxidase (HRP) conjugate was purchased from Promega (Madison, WI), and goat antimouse HRP conjugate was purchased from Jackson Immunoresearch Lab (West Grove, PA).

Perfluorooctanoic acid (PFOA), perfluorooctane sulfonic acid potassium salt (PFOSK), perfluorononanoic acid (PFNA), perfluorododecanoic acid (PFDoA), and perfluoroundecanoic acid (PFUnDA) were obtained from Sigma-Aldrich (St. Louis, MO). 1H,1H,2H,2H-Perfluorohexane sulfonic acid (4:2 FTS) and 1H,1H,2H,2H-perfluorodecane sulfonic acid (8:2 FTS) were obtained from Apollo Chemical Company. 1H,1H,2H,2H-Perfluorooctane sulfonic acid (6:2 FTS) and perfluoroheptane sulfonic acid (PFHpS) were obtained from SynQuest Laboratories (Alachua, FL). Perfluorohexane sulfonic acid (PFHxS) was obtained from LGC Standards USA (Manchester, NH). Perfluorodecane sulfonic acid (PFDS) was obtained from Toronto Research Chemicals (Toronto, ON). M8-PFOS and MPFOA, used as the internal standards, were obtained from Wellington Laboratories (Guelph, ON). All PFAS were dissolved in 100% methanol to obtain 10 mM individual stocks.

Coomassie protein assay reagent and albumin standard for the Bradford assay kit were purchased from Thermo Fisher Scientific (Waltham, MA). Dimethyl sulfoxide (DMSO) was obtained from Sigma-Aldrich (St. Louis, MO); sulfosuccinimidyl oleate (SSO) was obtained from Cayman Chemical (Ann Arbor, MI); 3-(4,5-dimethylthiazol-2-yl)-2,5-diphenyltetrazolium bromide (MTT) was obtained from Alfa Aesar (Haverhill, MA); LC-MS grade methanol was obtained from EMD Millipore (Billerica, MA); lipofectamine and P3000 reagent were obtained from Invitrogen (Waltham, MA); and Opti-MEM was obtained from Thermo Fisher (Waltham, MA). Liquid chromatography mass spectrometry (LC-MS) column and guard column were obtained from Phenomenex (Torrence, CA). Mass Hunter Qualitative Analysis (version 06.00), which was utilized for data analysis, was obtained from Agilent Technologies (Santa Clara, CA).

METHODS

Cell Culture. hTERT RPE-1 cells were grown in Dulbecco's modified Eagle's medium/nutrient mixture F-12 (DMEM/F-12) supplemented with L-glutamine and 15 mM HEPES. HEK-293T cells were grown in Dulbecco's modified Eagle's medium (DMEM) supplemented with 4.5 g/L glucose and L-glutamine without sodium pyruvate. Both growth media were supplemented with 10% (v/v) FBS and 1% (v/v) penicillin–streptomycin. Cells were grown at 37 °C and 5% $\rm CO_2$ atmosphere until they reached 80–90% confluency for use.

PFAS Treatment. hTERT RPE-1 cells (2.5×10^6) were seeded on 10 cm Petri dishes containing complete growth medium and incubated for 24 h prior to PFAS treatment; 4:2 FTS, 6:2 FTS, 8:2 FTS, PFHxS, PFOS, PFDS, PFOA, PFNA, PFUnDA, and PFDoA at 1 mM individually and as a mixture was prepared (10 mM total PFAS in mixture) in MeOH and spiked into the plates (n = 3) to obtain a final concentration of 10 μ M individually (and 100 μ M PFAS in mixture) and 1% MeOH (v/v). Cells were also treated with the same PFAS mixture to obtain a final concentration of 10 μM PFAS (1 μM each PFAS) for 24 h with 1% MeOH (v/v) as a control. Cell pellets from 10 cm \times 10 cm plates containing 2.5 \times 10⁶ hTERT RPE-1 cells each were also grown and treated with 1% MeOH (v/v) as a vehicle control and to prepare a calibration curve for the quantification of PFAS. After a 24 h treatment, cells were collected and centrifuged at 500g for 5 min at 4 °C. The media was then decanted, and the cell pellet was washed and resuspended with cold phosphate-buffered saline (PBS) and centrifuged under the same conditions to remove any remaining media. The cell pellet was resuspended in 1 mL cold PBS, and 30 μ L aliquot of the cell suspension was then taken and mixed with an equal volume of lysis buffer and incubated on ice for an hour. The protein concentration of each sample was determined using a Bradford protein assay. The cell pellet containing the remaining 970 μ L of PBS was centrifuged again at the same conditions, and the PBS

was removed. The cell pellets were stored at -80 $^{\circ}\text{C}$ until the PFAS extraction was performed.

Cell Viability Assay. Cell viability was measured using an MTT assay. 31 For the MTT assay, hTERT RPE-1 cells were seeded in 96well plates with 5000 cells per well for 24 h prior to the addition of PFAS treatments. After 24 h of attachment, 50 μ L of individual PFAS at various concentrations (1-100 μ M), with a final MeOH concentration of 1% (v/v), was added to each well (n = 5). After a 24 h PFAS treatment, the 96-well plate was centrifuged at 200g at 25 °C for 2 min. The complete growth media was aspirated and was replaced with 200 µL of fresh media containing 0.5 mg/mL of MTT reagent. The plate was then incubated at 37 °C for 2.5 h and centrifuged at 200g at 25 °C for 2 min. After centrifugation, 155 μ L of media containing the MTT reagent was removed and 90 µL of DMSO was added to each well. Each well was resuspended to improve the solubilization of the formazan, centrifuged at 1000g at 25 °C for 1 min, and then incubated at 37 °C for 10 min. Absorbance was measured using a Bio-Tek Synergy H1 plate reader at 550 nm. To calculate the percent viability of the treated compared to that of the control cells, the raw absorbance of cells was subtracted from the average absorbance of the blanks, which only contained MTT reagent (n = 5). All of the corrected absorbance values of the treated cells (n = 5)5) were then normalized to the methanol-treated samples (n = 5) and expressed as percent cell viability.

PFAS Extraction from Cell Lysates. For PFAS extraction, the cell pellets treated with PFAS along with vehicle control were resuspended in 1 mL of cold MeOH and vortexed for 30 s. The cell suspension was then sonicated at 40% power three times for 10 s while on a cold metal block. After sonication, the samples were centrifuged (16,000g, 15 min, 4 °C). The supernatant was then transferred to a 1 dram glass vial without disrupting the cell pellet. The cell pellet was then resuspended in 1 mL of cold MeOH, the extraction was repeated, and the supernatant was combined with the supernatant from the first extraction. The supernatant was then dried under vacuum. The samples were normalized based on their previously obtained protein concentration and resuspended in MeOH $\geq 150~\mu L$ spiked with 500 nM M8-PFOS and 500 nM MPFOA to be used as internal standards.

Preparation of Calibration Curves. The cell pellets, which were treated in 1% (v/v) MeOH for the calibration curve, were combined and resuspended in cold MeOH. Six 1 mL aliquots of cold MeOH were placed in six separate centrifuge tubes with one tube spiked with the PFAS mixture to obtain a concentration of 500 nM PFAS (5 μ M total PFAS) after extraction and resuspension. The PFAS-spiked sample after resuspension in MeOH containing the internal standard was then serially diluted 1:2 with the five nonspiked samples to obtain a calibration curve for quantification using MeOH containing the internal standard. The calibration curve range of 500-15.6 nM was used to avoid carryover. We note that, for this reason, PFAS-treated samples (n = 3) after resuspension were diluted $10 \times$ and $100 \times$ prior to LC-MS analysis (see the PFAS Extraction from Cell Lysates section for sample preparation). Internal standard-corrected calibration curves were prepared along with limits of detection (LODs)/limits of quantification (LOQs) for each PFAS (Supporting Information).

LC-MS Data Acquisition. LC-MS analyses were carried out in negative mode using an Agilent 1260 HPLC in tandem with an Agilent 6530 Jet Stream ESI-QToF-MS system with a Gemini C18 reverse-phased column (5 μ M, 4.6 mm \times 50 mm, Phenomenex). Mobile phase A was composed of 5 mM ammonium acetate in water with pH adjusted to 3.80. Mobile phase B was 100% MeOH. The gradient for PFAS elution and separation began with 50% B at 0.5 mL/min and after 5 min increasing to 95% B until 15 min. It was then held at 95% B until 30 min and then switched back to 50% B until 35 min for equilibration. The capillary voltage was set to 3500 V with the fragmentor voltage set to 175 V. The drying gas temperature was set to 350 °C with the flow rate set to 12 L/min. All PFAS were detected in negative mode as [M-H]⁻.

Cellular Distribution of PFAS. hTERT RPE-1 cells were grown, treated with the PFAS mixtures, and collected. The protein concentrations were measured prior to freezing the pellets. The

pellets were then thawed on ice and resuspended with a cold PBS-containing protease inhibitor with volumes based on their protein concentration and sonicated on a cold block. The samples were then transferred to 1 mL ultracentrifuge tubes and centrifuged at 100,000g at 4 °C for an hour to separate soluble (cytosolic) and insoluble (membrane and nuclear debris) components. The supernatant was transferred to a separate centrifuge tube and dried under nitrogen overnight. The insoluble and the dried cytosolic fraction were then extracted with MeOH, dried, and resuspended with 150 μ L methanol containing 500 nM M8-PFOS and MPFOA. Samples were analyzed via LC-MS using the previously described method in the LC-MS Data Acquisition section, undiluted and 10× diluted.

CD36 Overexpression in HEK-293T Cells. Plasmid transfection was carried out using the procedure given in the Invitrogen transfection kit with 7.5 μ L lipofectamine and 2.5, 1.25, and 0.625 μ g plasmids added. Lipofectamine only was added to n=3 wells as a control, while n=3 wells contained both plasmid and lipofectamine. To determine transfection efficiency, cells were also plated and treated with plasmid and lipofectamine on two glass-bottom Petri dishes (lipofectamine control and transfected) for fluorescence imaging. The 6-well plate and glass-bottom Petri dishes were incubated at 37 °C for 24 h after transfection. After a 24 h transient overexpression, the media was removed from the glass-bottom Petri dishes and carefully washed 2× with 2 mL PBS and left in 1 mL PBS. Imaging was carried out on Leica DMI6000B inverted software using LAS AF software (Leica AF6000 Modular System).

Inhibition of CD36 Using SSO in HEK-293T Cells. A 20 mM stock solution of SSO was prepared in DMSO. Final treatment conditions contained 0.5% DMSO. Twenty-four hours after transfection, CD36-overexpressing and control cells were treated with a 10 μ M PFAS mixture (1 μ M each PFAS) in the presence or absence of 100 μ M SSO. Cells were then collected, extracted, and analyzed as previously described.

Western Blot Analysis. Frozen cell pellets were thawed and lysed using MPER lysis buffer. The cell lysates were then centrifuged at 4 °C for 15 min at 16,000g, and then the supernatant was collected for analysis. Protein concentrations were determined via Bradford protein assay. Proteins were then normalized based on their protein concentrations and then diluted 1:1 with a solution containing 95% Laemmli buffer and 5% 2-mercaptoethanol and then placed on a heat block at 90 °C for 4 min and then stored at −20 °C prior to use. Equivalent amounts of protein were then loaded on 10% polyacrylamide gels and were separated via SDS-PAGE and transferred to a PDVF membrane. Membranes were washed with tris-buffered saline (TBS)-Tween (20 mM tris-base, 150 mM NaCl, pH 7.50 with 0.2% v/v Tween-20) and blocked with a solution of 5% w/v nonfat milk powder dissolved in TBS-Tween for 1 h. Membranes were then washed 3× with TBS-Tween for 10 min prior to incubation in a primary antibody (anti-CD36 or anti- α tubulin) for 16 h at 4 °C. Membranes were then washed 3× with TBS-Tween for 10 min and incubated with an anti-rabbit or antimouse HRP-conjugated secondary antibody diluted in 5% milk in TBS-Tween for 1 h at room temperature. Membranes were developed using the Super Signal West Pico kit using the manufacturer's guidelines. Membranes were imaged using a Bio-Rad ChemiDoc Imaging System.

■ RESULTS AND DISCUSSION

PFAS-Induced Toxicity in Human Epithelial Cells. To investigate the cytotoxic effects of PFAS, we used a broad range of compounds, which varied in chain length (4:2 FTS vs 6:2 FTS vs 8:2 FTS or PFHxS vs PFHpS vs PFOS vs PFDS), degree of fluorination (6:2 FTS vs PFOS, or 8:2 FTS vs PFDS), and head group (PFOS vs PFOA). Specifically, we focused on 6–10 carbon-containing PFAS with carboxylate and sulfonate head groups. We also included fluorotelomer PFAS, which are structurally similar to sulfonate PFAS with the exception that they lack fluorination in the 1,2 positions on the

alkyl backbone (Figure 1A). The toxicity analysis was carried out in immortalized retinal pigment epithelial cells, hTERT RPE-1, using 3-(4,5-dimethylthiazol-2-yl)-2,5-diphenyltetrazolium bromide (MTT) cell viability assays.³¹ This cell line was chosen due to its noncancerous nature and its ability to undergo extensive population doublings. To assess PFAS toxicity, we carried out MTT assays using a range of concentrations (1–100 μ M) after a 24 h exposure. Figure 1B summarizes the cell viability data that we obtained (see Table S1 for detailed representation). There were no significant changes in cell viability with the treatment of PFAS with carboxylate head groups (i.e., PFOA, PFUnDA, PFDoA) ranging from 8 to 12 carbons with the exception of PFNA, which induced $\sim 30\%$ toxicity at 30 and 100 μM (Figure 1B). These findings are consistent with previous studies that reported toxicity at high concentrations (≥ 250 μ M). At low concentrations (up to 10 μ M), PFOA and PFDoA slightly promoted cell viability. Interestingly, similar to PFOA and PFDoA, PFOS induced slight increases in cell viability at all of the concentrations tested, up to 100 μ M. Pierozan et al. also reported a similar prosurvival effect of PFOS,²⁴ which could be linked to the high bioaccumulative potential of PFOS.³² Both the sulfonate and fluorotelomer PFAS showed a trend of increasing toxicity with increasing chain length. The shorter-chained sulfonates and fluorotelomers (i.e., 6-8 carbons in length) did not show any toxicity at any of the concentrations tested. These results suggest that fluorotelomers exhibit similar, if not higher, levels of toxicity, which will be important for future studies prioritizing these classes of PFAS for their adverse effects. One striking difference we observed was that 8:2 FTS exhibited increased toxicity relative to its fully fluorinated counterpart (PFDS) at 10 and 30 μ M. At 100 μ M, both 8:2 FTS and PFDS caused an ~50% decrease in cell viability (Figure 1B).

Uptake of PFAS with Varying Chain Length, Degree of Fluorination, and Head Group. To investigate whether the differences in toxicity we observed could be due to the differences in their cellular uptake, we first measured the levels of select PFAS in hTERT RPE-1 cells. Based on the differences in cell viability we observed for fluorotelomer PFAS and their fully fluorinated forms, we focused on PFHxS, PFOS, PFDS, 4:2 FTS, 6:2 FTS, and 8:2 FTS for these uptake experiments but also included carboxylates (PFOA, PFNA, PFUnDA, and PFDoA) to determine if head group differences can also affect uptake. Using similar treatment conditions reported in the PFAS-Induced Toxicity in Human Epithelial Cells section, we treated hTERT RPE-1 cells with 10 μ M PFAS individually for 24 h. Since PFAS are found as mixtures in the environment,³³ we also investigated their uptake when cells are exposed to a mixture of PFAS (10 and 1 µM for each PFAS resulting in a total of 100 and 10 μ M PFAS) to compare the differences in uptake when present as a mixture vs individually. We collected PFAS-exposed hTERT RPE-1 pellets and extracted PFAS using MeOH extraction (see the PFAS Extraction from Cell Lysates section). The extraction efficiencies are reported in Table S2. We then measured the levels of PFAS in cellular extracts using LC-MS. Using matrix-matched calibration curves (Figure S1), we calculated their concentrations with limits of detection (LODs) and quantification (LOQs), which varied from 0.1 to 3.3 nM and 0.4 to 11 nM, respectively (Table S3).

When PFAS were presented as a mixture, only the longerchained PFAS of each class (6:2 FTS, PFOS, 8:2 FTS, PFDS,

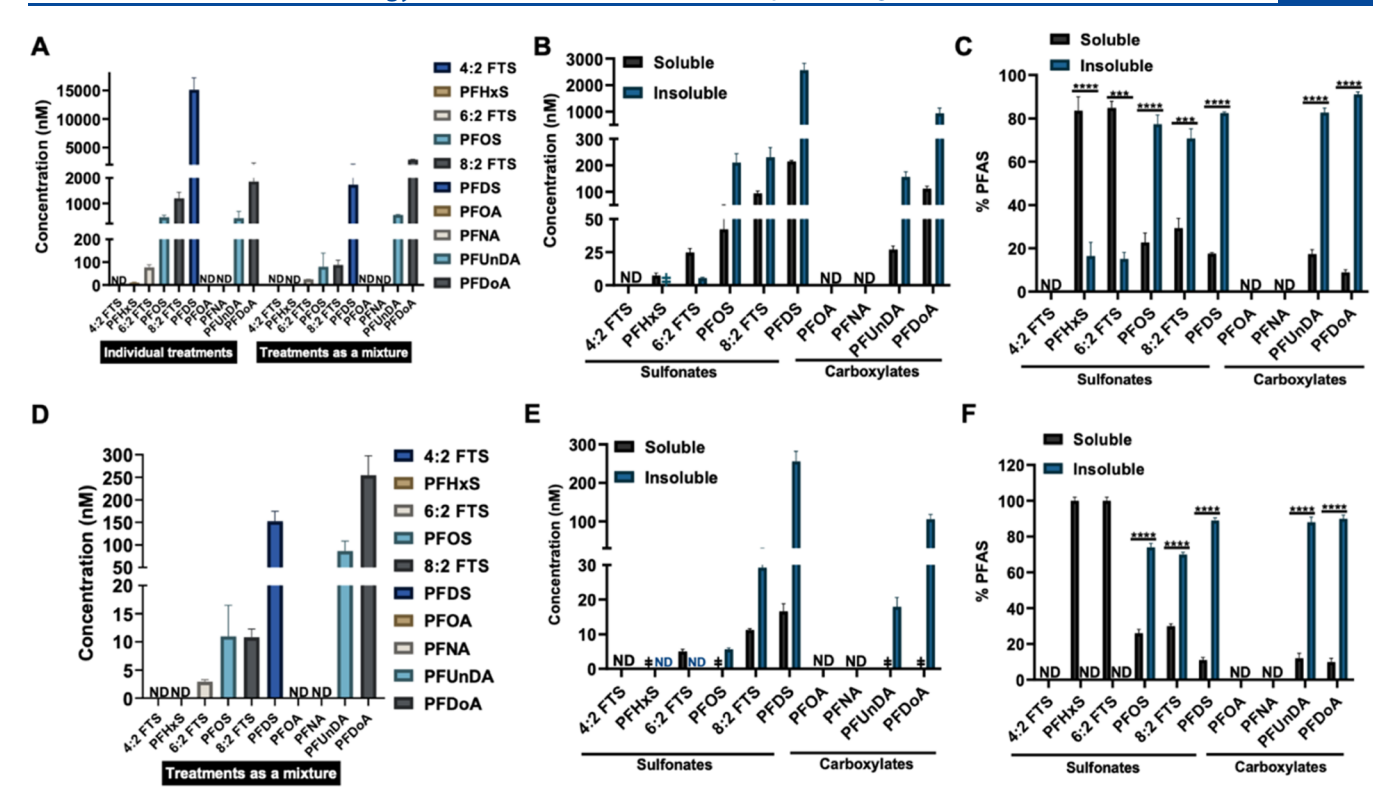


Figure 2. Cellular uptake and distribution of PFAS. (A) Concentrations of different PFAS in hTERT RPE-1 cell extracts obtained from treatments with 100 μ M PFAS (10 μ M each) in a mixture or individually for 24 h. Concentrations in the extracts are calculated using a calibration curve in the cell matrix, which was prespiked with PFAS prior to MeOH extraction. (B, C) Levels of PFAS in soluble and insoluble compartments of hTERT RPE-1 cells treated with the PFAS mixture (10 μ M each of PFAS). (B) Concentrations of PFAS detected in each extract. Each extract corresponded to the cellular material from ~2.5 × 10⁶ cells. (C) Percent PFAS present within each fraction. (D) Concentrations of different PFAS in hTERT RPE-1 cell extracts obtained from treatments with 10 μ M PFAS (1 μ M each) in a mixture for 24 h. Concentrations in the extracts are calculated using a calibration curve in the cell matrix, which was prespiked with PFAS prior to MeOH extraction. (E, F) Levels of PFAS in soluble and insoluble compartments of hTERT RPE-1 cells treated with 10 μ M PFAS mixture (1 μ M each PFAS). (E) Concentrations of PFAS detected in each extract. Each extract corresponded to the cellular material from ~2.5 × 10⁶ cells. (F) Percent PFAS present within each fraction. ND, not detected; \ddagger , detected, <LOQ; ****p-value ≤ 0.001; *****p-value ≤ 0.0001.

PFUnDA, and PFDoA) were detected, while the other shorterchained PFAS (4:2 FTS, PFHxS, PFOA, and PFNA) were below the LODs. PFAS concentrations in the extracts ranged from ~ 0.025 to 3 μ M with increasing chain length (~ 0.025 and 3 µM for 6:2 FTS and PFDoA, respectively; Figure 2A) for the 100 μ M total PFAS mixture and ~3-255 nM for the 10 μ M total PFAS mixture (Figure 2D). We also note that the uptake of PFAS, except 6:2 FTS, is time-dependent where the uptake increases over time (4–16 h; Figure S2). For individual treatments at 10 µM, we observed similar trends: PFHxS was present at low levels (<LOD for 4:2 FTS, PFOA, and PFNA, and 10 nM for PFHxS), whereas 6:2 FTS, 8:2 FTS, PFOS, PFDS, PFUnDA, and PFDoA showed strong associations with cells (Figure 2A). Based on the concentrations detected in the extracts, a number of key observations emerged. First, the degree of fluorination can be an important factor for uptake since the fully fluorinated PFAS were present in the cell at higher concentrations compared to their fluorotelomer counterparts when present individually and as a mixture. Second, our results suggest that the differences in the head group contribute to cellular uptake as sulfonates are taken up at higher levels compared to carboxylates of the same chain length (i.e., ~450 nM for PFOS vs not detected for PFOA). Third, higher cellular concentrations were measured with increasing carbon number in the fluorotelomers, sulfonates, and carboxylates that we tested. Furthermore, we also note the

decreased uptake of certain PFAS when presented as a mixture: 4:2 FTS and PFHxS were not detected in the cell in either condition, and 6:2 FTS was detected in cells that were treated individually but at very low concentrations with almost a 100fold difference (<10 nM) compared to the other PFAS tested (Figure 2A,D). Overall, our data suggests that, among the PFAS tested, their cellular uptake increases with chain length and fully fluorinated sulfonates are taken up more effectively as compared to their fluorotelomer and carboxylate counterparts. Previous studies investigated the cellular uptake of various carboxylates and shorter-chained sulfonates in HepG2 cells. Our results are consistent with these findings, which showed an increase in PFAS uptake for carboxylates based on chain length. 28,29 One difference we note is that Rosenmai et al. reported enhanced uptake for PFHxS as compared to that for PFOS in HepG2 cells. However, the difference in cellular uptake data is limited in explaining the increased toxicity of 8:2 FTS as compared to that of PFDS (Figure 1B) and suggests that interactions with specific biomolecules based on the precise PFAS structure could be responsible for differential effects on cell viability.

Cellular Distribution of PFAS. Since PFAS have a hydrophobic tail and can show a strong association with biological membranes, we next investigated the levels of PFAS in hTERT RPE-1 cells in soluble (cytoplasmic) and insoluble (membrane and nuclear debris) fractions. We treated cells with

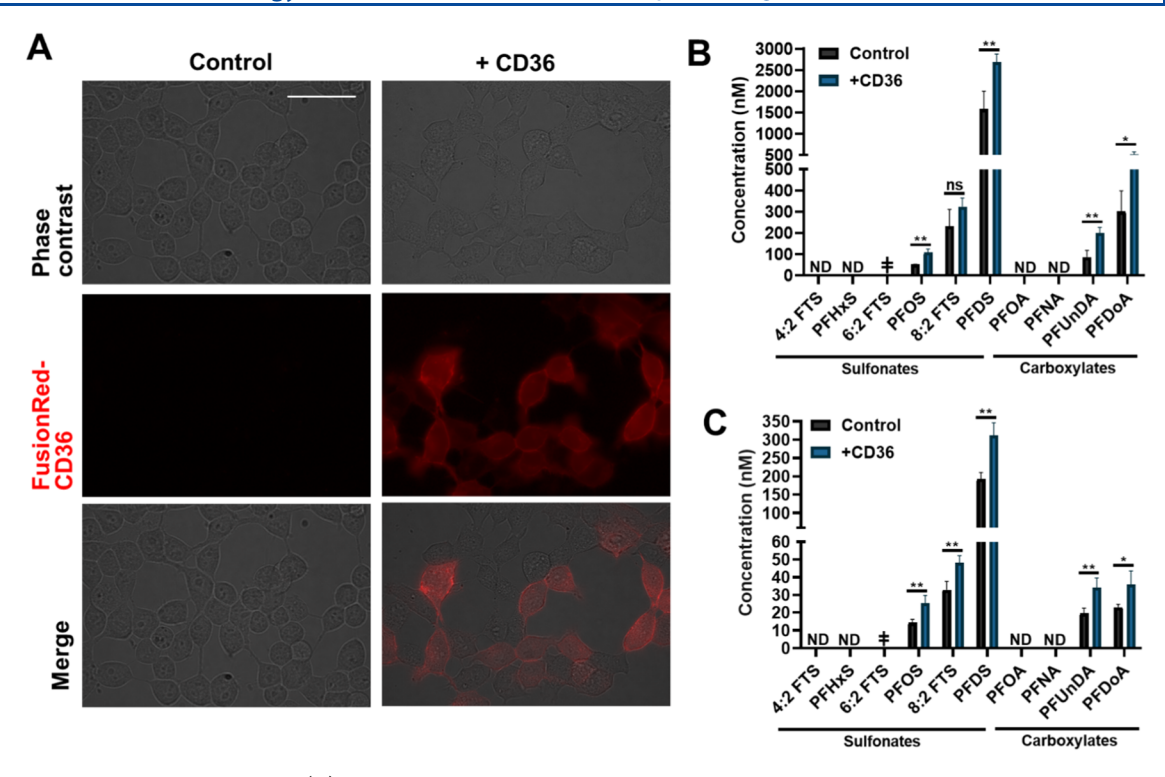


Figure 3. Role of CD36 in PFAS uptake. (A) Overexpression of FusionRed-CD36 in HEK-293T cells. Overexpression was allowed for 24 h and provided a transfection efficiency of $71 \pm 8\%$ (n = 3, 120 cells analyzed). (B, C) Concentration of PFAS within CD36-overexpressing HEK-293T cells (n = 3) compared to that of control cells at 6 h treatment times. Cells were incubated overnight at 37 °C. After 24 h, the CD36 plasmid with lipofectamine was added to the cells along with lipofectamine only as a control and allowed to overexpress CD36 for 24 h prior to PFAS treatment. Cells were then treated with the (B) 100 μ M PFAS mixture (10 μ M each) or (C) 10 μ M PFAS mixture (1 μ M each) for 6 h prior to cell collection. The levels in cell extracts that are normalized based on the protein content are reported. ND, not detected; ‡, detected, <LOQ; *p-value \leq 0.05, *p-value \leq 0.01.

PFAS as described in the Uptake of PFAS with Varying Chain Length, Degree of Fluorination, and Head Group section with the 100 and 10 μ M PFAS mixture separately for 24 h (10 and 1 μ M 4:2 FTS, 6:2 FTS, 8:2 FTS, PFHxS, PFOS, PFDS, PFOA, PFNA, PFUnDA, and PFDoA each), fractionated soluble and insoluble components using ultracentrifugation, and analyzed the levels of PFAS. Figure 2B,E shows the concentration of PFAS detected in each extract for 100 and 10 µM mixtures, respectively. The relative abundances of each PFAS for 100 and 10 μ M mixtures are shown in Figure 2C,F for the ease of comparison. In these mixtures, we were able to detect one of the shorter-chained PFAS (i.e., PFHxS) in the soluble (cytosolic) fraction (Figure 2B,E); 6:2 FTS was mostly (>85%) detected in the soluble fraction and was at much lower levels compared to the five other longer-chained PFAS (Figure 2B,E). Other PFAS were primarily detected in the insoluble (membrane and nuclear debris) fraction as compared to that in the soluble fraction, with 90% of PFDS, PFUnDA, and PFDoA being present in the insoluble fraction (Figure 2C,F).

Our results suggest that carbon chain length, degree of fluorination, and head group play a role in the cellular distribution of PFAS. Based on the species analyzed, it seems longer-chained PFAS show stronger association with the insoluble fraction. For example, both PFDS and 8:2 FTS are present at higher levels in the insoluble fraction as compared to their shorter-chained versions, PFOS and 6:2 FTS, respectively. Meanwhile, PFHxS and 6:2 FTS were mostly detected in the soluble fraction. In parallel, fully fluorinated PFAS show higher association with the insoluble fraction, with 6:2 FTS primarily detected in the soluble fraction and >85% of PFOS

being in the insoluble fraction (Figure 2C,F). These trends in the PFAS uptake could be due to multiple mechanisms: the longer-chained PFAS strongly associating with cell membranes due to their hydrophobicity or the involvement of active transport mechanisms that are at play for the uptake of longer-chained PFAS.

CD36, a Fatty Acid Transporter, Is Involved in the Uptake of PFAS. Our results show that longer-chained PFAS are taken up more effectively into cells, which suggests that active transport might play a role in their uptake as opposed to passive diffusion. Previous work by Wu et al. showed transcriptional upregulation of the fatty acid transporter CD36 upon exposure to PFOA in mouse liver.³⁰ Based on our findings and the literature, we hypothesized that CD36 can be involved in the uptake of PFAS and decided to investigate its role in PFAS uptake using an overexpression system of CD36 in HEK-293T cells. We chose HEK-293T cells due to their high transfection efficiency.³⁴ First, we determined the levels of PFAS under similar treatment conditions using LC-MS in HEK-293T cells (see Figure S3 for matrix-matched calibration curves and Figure S4 and Table S3 for concentrations in extracts along with their LOD/LOQs). We found that longer-chained PFAS (PFDS, 8:2 FTS, PFUnDA, and PFDoA) are taken up almost 10× higher as compared to shorter-chained versions (PFOS and 6:2 FTS, respectively, and PFOA and PFNA below LODs) similar to our observations in hTERT RPE-1 cells, making HEK-293T a suitable cell line for these experiments. We transiently overexpressed a fluorescently tagged version of CD36 (FusionRed-CD36) for 24 h in HEK-293T with a transfection efficiency of $71 \pm 8\%$ (Figure

3A and see Figure S5 for Western blot using varying amounts of plasmid during transfection). We then treated CD36overexpressing and control cells with the PFAS mixtures (10 and 100 μ M) for 6 h. This PFAS treatment time was chosen because prolonged overexpression of CD36 induces toxicity in HEK-293T cells (data not shown). Similar to what we observed in hTERT RPE-1 cells, the shorter-chained PFAS, PFHxS and 4:2 FTS, were not detected in any of the conditions, and 6:2 FTS was detected below the LOQ (Figure 3B,C). Interestingly, for the PFAS that were detected in the extracts, CD36 overexpression resulted in higher levels at both concentrations of the mixtures (see Table S4 for individual values) compared to the control. Specifically, CD36-overexpressing HEK-293T cells showed 1.4-2.3-fold higher levels of PFAS for the 100 μ M PFAS mixture and 1.6-1.8-fold higher levels for the 10 μ M PFAS mixture (p < 0.05; Figure 3B,C) compared to those of the control.

To validate the involvement of CD36 in PFAS uptake, we treated CD36-overexpressing HEK-293T cells with sulfosuccinimidyl oleate (SSO), a commonly used CD36 inhibitor. 35-37 Prior to PFAS treatment, CD36-overexpressing and control cells were treated with either 100 μ M SSO or 0.5% DMSO as vehicle control. Cells were exposed to a 10 μ M PFAS mixture as described earlier, and PFAS levels were analyzed. SSO treatment significantly decreased the levels of PFAS that were detected in the extracts (i.e., PFOS, 8:2 FTS, PFDS, PFUnDA, PFDoA), albeit to different extents (Figure S6). These results support that increased CD36 levels result in the enhanced uptake of PFAS, linking the activity of this fatty acid transporter to PFAS uptake. Studies have shown that exposure to PFOA and other PFAS resulted in significant changes in lipid metabolism^{38,39} and membrane remodeling^{40,41} in cells, suggesting that these compounds might perturb lipid homeostasis in cells. Based on these results, it is plausible to envision that these compounds can undergo similar interactions with hydrophobic metabolites, primarily fatty acids and other lipids, and might perturb lipid homeostasis and production in cells.

CONCLUSIONS

Our results demonstrate that subtle differences in the chemical structures of PFAS can lead to different biomolecular interactions in vitro. We showed that head group, degree of fluorination, and chain length affect the cellular uptake of PFAS, with sulfonates exhibiting stronger cellular uptake as compared to fluorotelomer and carboxylate counterparts and PFAS of the same classes exhibiting stronger cellular uptake with increasing chain length. Furthermore, our results also provide evidence that the level of cellular uptake of PFAS can be different when they are present individually in solution as compared to when they are presented in a mixture. Finally, our results link a fatty acid transporter to the cellular uptake of PFAS. The results from this study will pave the way for studies on the behavior and interactions of PFAS within biological systems in vitro. In the future, comprehensive investigations that evaluate the bioactivity of a wider range of PFAS species that allow systematic comparisons and potential synergistic and antagonistic effects between PFAS in mixtures will lead the way to a better understanding of how these compounds interact with biological systems.

ASSOCIATED CONTENT

5 Supporting Information

The Supporting Information is available free of charge at https://pubs.acs.org/doi/10.1021/acs.chemrestox.2c00078.

Table of the viability results in PFAS-treated hTERT RPE-1 cells; table of the extraction efficiencies of PFAS; table of the limits of detection (LODs) and quantifications (LOQs) for hTERT RPE-1 and HEK-293T cells; table of the concentrations of PFAS within CD36-overexpressing HEK-293T cells compared to those of control cells at 6 h treatment times; matrix-matched internal standard-corrected calibration curves in hTERT RPE-1; heatmap representation of PFAS levels in hTERT RPE-1 cells with varying treatment times; matrix-matched internal standard-corrected calibration curves in HEK-293T cells; PFAS uptake in HEK293-T cells; Western blot for CD36 overexpression using varying amounts of plasmids; and the effect of SSO on the PFAS uptake (PDF)

AUTHOR INFORMATION

Corresponding Author

G. Ekin Atilla-Gokcumen — Department of Chemistry, University at Buffalo, The State University of New York (SUNY), Buffalo, New York 14260, United States; orcid.org/0000-0002-7132-3873; Email: ekinatil@buffalo.edu

Authors

Michelle Camdzic — Department of Chemistry, University at Buffalo, The State University of New York (SUNY), Buffalo, New York 14260, United States; occid.org/0000-0002-9928-1070

Diana S. Aga — Department of Chemistry, University at Buffalo, The State University of New York (SUNY), Buffalo, New York 14260, United States; orcid.org/0000-0001-6512-7713

Complete contact information is available at: https://pubs.acs.org/10.1021/acs.chemrestox.2c00078

Notes

The authors declare no competing financial interest.

ACKNOWLEDGMENTS

The authors gratefully acknowledge the support from the National Science Foundation (CBET-2112201). Any opinions, findings, conclusions, and recommendations expressed in this publication are those of the author(s) and do not necessarily reflect the view of the National Science Foundation.

REFERENCES

- (1) Centers for Disease Control and Prevention. Per- and Polyfluorinated Substances (PFAS) Factsheet. http://www.cdc.gov (accessed August 16, 2021).
- (2) Buck, R. C.; Franklin, J.; Berger, U.; Conder, J. M.; Cousins, I. T.; de Voogt, P.; Jensen, A. A.; Kannan, K.; Mabury, S. A.; van Leeuwen, S. P. Perfluoroalkyl and polyfluoroalkyl substances in the environment: Terminology, classification, and origins. *Integr. Environ. Assess. Manage.* **2011**, *7*, 513–541.
- (3) Cousins, E. M.; Richter, L.; Cordner, A.; Brown, P.; Diallo, S. Risky business? Manufacturer and retailer action to remove per-and polyfluorinated chemicals from consumer products. *New Solut.: J. Environ. Occup. Health Policy* **2019**, *29*, 242–265.

- (4) U.S. Environmental Protection Agency. Basic Information on PFAS. http://www.epa.gov (accessed August 15, 2021).
- (5) Barzen-Hanson, K. A.; Roberts, S. C.; Choyke, S.; Oetjen, K.; McAlees, A.; Riddell, N.; McCrindle, R.; Ferguson, P. L.; Higgins, C. P.; Field, J. A. Discovery of 40 classes of per-and polyfluoroalkyl substances in historical aqueous film-forming foams (AFFFs) and AFFF-impacted groundwater. *Environ. Sci. Technol.* **2017**, *51*, 2047–2057.
- (6) D'eon, J. C.; Mabury, S. A. Production of perfluorinated carboxylic acids (PFCAs) from the biotransformation of polyfluoroalkyl phosphate surfactants (PAPS): exploring routes of human contamination. *Environ. Sci. Technol.* **2007**, 41, 4799–4805.
- (7) Olsen, G. W.; Burris, J. M.; Ehresman, D. J.; Froehlich, J. W.; Seacat, A. M.; Butenhoff, J. L.; Zobel, L. R. Half-life of serum elimination of perfluorooctanesulfonate, perfluorohexanesulfonate, and perfluorooctanoate in retired fluorochemical production workers. *Environ. Health Perspect.* **2007**, *115*, 1298–1305.
- (8) Zhang, Y.; Beesoon, S.; Zhu, L.; Martin, J. W. Biomonitoring of perfluoroalkyl acids in human urine and estimates of biological half-life. *Environ. Sci. Technol.* **2013**, *47*, 10619–10627.
- (9) Post, G. B.; Cohn, P. D.; Cooper, K. R. Perfluorooctanoic acid (PFOA), an emerging drinking water contaminant: a critical review of recent literature. *Environ. Res.* **2012**, *116*, 93–117.
- (10) Reade, A.; Quinn, T.; Schreiber, S. Scientific and Policy Assessment for Addressing Per-and Polyfluoroalkyl Substances (PFAS) in Drinking Water; Natural Resources Defense Council: Lansing, MI, USA, 2019.
- (11) Olsen, G. W.; Mair, D. C.; Lange, C. C.; Harrington, L. M.; Church, T. R.; Goldberg, C. L.; Herron, R. M.; Hanna, H.; Nobiletti, J. B.; Rios, J. A.; et al. Per-and polyfluoroalkyl substances (PFAS) in American Red Cross adult blood donors, 2000–2015. *Environ. Res.* 2017, 157, 87–95.
- (12) Jian, J.-M.; Chen, D.; Han, F.-J.; Guo, Y.; Zeng, L.; Lu, X.; Wang, F. A short review on human exposure to and tissue distribution of per-and polyfluoroalkyl substances (PFASs). *Sci. Total Environ.* **2018**, *636*, 1058–1069.
- (13) Pérez, F.; Nadal, M.; Navarro-Ortega, A.; Fàbrega, F.; Domingo, J. L.; Barceló, D.; Farré, M. Accumulation of perfluoroalkyl substances in human tissues. *Environ. Int.* **2013**, *59*, 354–362.
- (14) Mamsen, L. S.; Björvang, R. D.; Mucs, D.; Vinnars, M.-T.; Papadogiannakis, N.; Lindh, C. H.; Andersen, C. Y.; Damdimopoulou, P. Concentrations of perfluoroalkyl substances (PFASs) in human embryonic and fetal organs from first, second, and third trimester pregnancies. *Environ. Int.* **2019**, *124*, 482–492.
- (15) Liu, G.; Dhana, K.; Furtado, J. D.; Rood, J.; Zong, G.; Liang, L.; Qi, L.; Bray, G. A.; DeJonge, L.; Coull, B.; Grandjean, P.; Sun, Q. Perfluoroalkyl substances and changes in body weight and resting metabolic rate in response to weight-loss diets: A prospective study. *PLoS Med* **2018**, *15*, No. e1002502.
- (16) Bach, C. C.; Vested, A.; Jørgensen, K. T.; Bonde, J. P. E.; Henriksen, T. B.; Toft, G. Perfluoroalkyl and polyfluoroalkyl substances and measures of human fertility: a systematic review. *Crit. Rev. Toxicol.* **2016**, *46*, 735–755.
- (17) Wan, H.; Zhao, Y.; Wong, M. H.; Lee, K.; Yeung, W.; Giesy, J.; Wong, C. Testicular signaling is the potential target of perfluor-octanesulfonate-mediated subfertility in male mice. *Biol. Reprod.* **2011**, *84*, 1016–1023.
- (18) Mitchell, R. J.; Myers, A. L.; Mabury, S. A.; Solomon, K. R.; Sibley, P. K. Toxicity of fluorotelomer carboxylic acids to the algae Pseudokirchneriella subcapitata and Chlorella vulgaris, and the amphipod Hyalella azteca. *Ecotoxicol. Environ. Saf.* **2011**, *74*, 2260–2267.
- (19) Phillips, M. M.; Dinglasan-Panlilio, M. J. A.; Mabury, S. A.; Solomon, K. R.; Sibley, P. K. Fluorotelomer acids are more toxic than perfluorinated acids. *Environ. Sci. Technol.* **2007**, *41*, 7159–7163.
- (20) Hoke, R. A.; Bouchelle, L. D.; Ferrell, B. D.; Buck, R. C. Comparative acute freshwater hazard assessment and preliminary PNEC development for eight fluorinated acids. *Chemosphere* **2012**, 87, 725–733.

- (21) Meneguzzi, A.; Fava, C.; Castelli, M.; Minuz, P. Exposure to perfluoroalkyl chemicals and cardiovascular disease: experimental and epidemiological evidence. *Front. Endocrinol.* **2021**, *12*, No. 850.
- (22) Lu, Y.; Meng, L.; Ma, D.; Cao, H.; Liang, Y.; Liu, H.; Wang, Y.; Jiang, G. The occurrence of PFAS in human placenta and their binding abilities to human serum albumin and organic anion transporter 4. *Environ. Pollut.* **2021**, 273, No. 116460.
- (23) Lu, A.; Disoma, C.; Zhou, Y.; Chen, Z.; Zhang, L.; Shen, Y.; Zhou, M.; Du, A.; Zheng, R.; Li, S.; et al. Protein interactome of the deamidase phosphoribosylformylglycinamidine synthetase (PFAS) by LC-MS/MS. *Biochem. Biophys. Res. Commun.* **2019**, *513*, 746–752.
- (24) Pierozan, P.; Karlsson, O. PFOS induces proliferation, cell-cycle progression, and malignant phenotype in human breast epithelial cells. *Arch. Toxicol.* **2018**, *92*, 705–716.
- (25) Mahapatra, C. T.; Damayanti, N. P.; Guffey, S. C.; Serafin, J. S.; Irudayaraj, J.; Sepúlveda, M. S. Comparative in vitro toxicity assessment of perfluorinated carboxylic acids. *J. Appl. Toxicol.* **2017**, 37, 699–708.
- (26) Mulkiewicz, E.; Jastorff, B.; Składanowski, A.; Kleszczyński, K.; Stepnowski, P. Evaluation of the acute toxicity of perfluorinated carboxylic acids using eukaryotic cell lines, bacteria and enzymatic assays. *Environ. Toxicol. Pharmacol.* **2007**, 23, 279–285.
- (27) Kudo, N.; Suzuki, E.; Katakura, M.; Ohmori, K.; Noshiro, R.; Kawashima, Y. Comparison of the elimination between perfluorinated fatty acids with different carbon chain length in rats. *Chem.-Biol. Interact.* **2001**, *134*, 203–216.
- (28) Li, C.-H.; Shi, Y.-L.; Li, M.; Guo, L.-H.; Cai, Y.-Q. Receptor-bound perfluoroalkyl carboxylic acids dictate their activity on human and mouse peroxisome proliferator-activated receptor γ . *Environ. Sci. Technol.* **2020**, *54*, 9529–9536.
- (29) Rosenmai, A. K.; Ahrens, L.; le Godec, T.; Lundqvist, J.; Oskarsson, A. Relationship between peroxisome proliferator-activated receptor alpha activity and cellular concentration of 14 perfluoroalkyl substances in HepG2 cells. *J. Appl. Toxicol.* **2018**, *38*, 219–226.
- (30) Wu, X.; Liang, M.; Yang, Z.; Su, M.; Yang, B. Effect of acute exposure to PFOA on mouse liver cells in vivo and in vitro. *Environ. Sci. Pollut. Res.* **2017**, *24*, 24201–24206.
- (31) Denizot, F.; Lang, R. Rapid colorimetric assay for cell growth and survival: modifications to the tetrazolium dye procedure giving improved sensitivity and reliability. *J. Immunol. Methods* **1986**, *89*, 271–277.
- (32) Cao, H.; Zhou, Z.; Wang, L.; Liu, G.; Sun, Y.; Wang, Y.; Wang, T.; Liang, Y. Screening of potential PFOS alternatives to decrease liver bioaccumulation: Experimental and computational approaches. *Environ. Sci. Technol.* **2019**, *53*, 2811–2819.
- (33) Schulz, K.; Silva, M. R.; Klaper, R. Distribution and effects of branched versus linear isomers of PFOA, PFOS, and PFHxS: A review of recent literature. *Sci. Total Environ.* **2020**, 733, No. 139186.
- (34) Backliwal, G.; Hildinger, M.; Hasija, V.; Wurm, F. M. Highdensity transfection with HEK-293 cells allows doubling of transient titers and removes need for a priori DNA complex formation with PEI. *Biotechnol. Bioeng.* **2008**, *99*, 721–727.
- (35) Harmon, C. M.; Luce, P.; Beth, A. H.; Abumrad, N. A. Labeling of adipocyte membranes by sulfo-N-succinimidyl derivatives of long-chain fatty acids: inhibition of fatty acid transport. *J. Membr. Biol.* **1991**, *121*, 261–268.
- (36) Mansor, L. S.; Sousa Fialho, M. D. L.; Yea, G.; Coumans, W. A.; West, J. A.; Kerr, M.; Carr, C. A.; Luiken, J. J.; Glatz, J. F.; Evans, R. D.; et al. Inhibition of sarcolemmal FAT/CD36 by sulfo-N-succinimidyl oleate rapidly corrects metabolism and restores function in the diabetic heart following hypoxia/reoxygenation. *Cardiovasc. Res.* **2017**, *113*, 737–748.
- (37) Coort, S. L.; Willems, J.; Coumans, W. A.; Van Der Vusse, G. J.; Bonen, A.; Glatz, J. F.; Luiken, J. J. Sulfo-N-succinimidyl esters of long chain fatty acids specifically inhibit fatty acid translocase (FAT/CD36)-mediated cellular fatty acid uptake. *Mol. Cell. Biochem.* **2002**, 239, 213–219.

- (38) Wen, Y.; Mirji, N.; Irudayaraj, J. Epigenetic toxicity of PFOA and GenX in HepG2 cells and their role in lipid metabolism. *Toxicol. In Vitro* **2020**, *65*, No. 104797.
- (39) Peropadre, A.; Hazen, M. J.; Martín, J. M. P.; Freire, P. F. An acute exposure to perfluorooctanoic acid causes non-reversible plasma membrane injury in HeLa cells. *Environ. Pollut.* **2020**, 260, No. 114008.
- (40) Aristizabal-Henao, J. J.; Ahmadireskety, A.; Griffin, E. K.; Da Silva, B. F.; Bowden, J. A. Lipidomics and environmental toxicology: Recent trends. *Curr. Opin. Environ. Sci. Health* **2020**, *15*, 26–31.
- (41) Jantzen, C. E.; Annunziato, K. M.; Cooper, K. R. Behavioral, morphometric, and gene expression effects in adult zebrafish (*Danio rerio*) embryonically exposed to PFOA, PFOS, and PFNA. *Aquat. Toxicol.* **2016**, *180*, 123–130.

□ Recommended by ACS

Insights into the Competitive Mechanisms of Per- and Polyfluoroalkyl Substances Partition in Liver and Blood

Yibo Jia, Lingyan Zhu, et al.

APRIL 18, 2022

ENVIRONMENTAL SCIENCE & TECHNOLOGY

READ 🗹

Perfluoroalkyl Substances of Significant Environmental Concern Can Strongly Inhibit Human Carbonic Anhydrase Isozymes

Giang T. H. Nguyen, William A. Donald, et al.

FEBRUARY 25, 2020

ANALYTICAL CHEMISTRY

READ 🗹

Long-Chain Perfluoroalkyl acids (PFAAs) Affect the Bioconcentration and Tissue Distribution of Short-Chain PFAAs in Zebrafish (Danio rerio)

Wu Wen, Hui Lin, et al.

OCTOBER 09, 2017

ENVIRONMENTAL SCIENCE & TECHNOLOGY

READ 🗹

Screening of Potential PFOS Alternatives To Decrease Liver Bioaccumulation: Experimental and Computational Approaches

Huiming Cao, Yong Liang, et al.

FEBRUARY 08, 2019

ENVIRONMENTAL SCIENCE & TECHNOLOGY

READ 🗹

Get More Suggestions >